Three-dimensional localization precision of the double-helix point spread function versus astigmatism and biplane

Majid Badieirostami,[1] Matthew D. Lew,[1,2] Michael A. Thompson,[1] and W. E. Moerner[1,a)]
[1]*Department of Chemistry, Stanford University, Stanford, California 94305, USA*
[2]*Department of Electrical Engineering, Stanford University, Stanford, California 94305, USA*

(Received 2 June 2010; accepted 21 September 2010; published online 18 October 2010)

Wide-field microscopy with a double-helix point spread function (DH-PSF) provides three-dimensional (3D) position information beyond the optical diffraction limit. We compare the theoretical localization precision for an unbiased estimator of the DH-PSF to that for 3D localization by astigmatic and biplane imaging using Fisher information analysis including pixelation and varying levels of background. The DH-PSF results in almost constant localization precision in all three dimensions for a 2 μm thick depth of field while astigmatism and biplane improve the axial localization precision over smaller axial ranges. For high signal-to-background ratio, the DH-PSF on average achieves better localization precision. © *2010 American Institute of Physics*.
[doi:10.1063/1.3499652]

Over the past half century, fluorescence microscopy has emerged to become one of the most widely used tools in biological research.[1] In spite of the major advantages of noninvasive imaging and molecular labeling specificity, the spatial resolution for visible wavelengths is limited by the diffraction of light to about 300 nm in the lateral dimensions. In order to circumvent the diffraction limit, various superresolution (SR) imaging techniques based on sequential wide-field imaging of sparse single-molecule emitters have been developed. Among these methods, fluorescence photoactivated localization microscopy (PALM, F-PALM) (Refs. 2 and 3) and stochastic optical reconstruction microscopy (STORM) (Ref. 4) have achieved more than one order of magnitude higher two-dimensional (2D) spatial resolution in cellular studies. Although these techniques have improved 2D performance, axial (z) SR is also necessary for complete and meaningful investigation of most cellular structures. Unfortunately, the three-dimensional (3D) point spread function (PSF) of the standard fluorescence microscope is not well-suited for 3D SR imaging for two reasons. First, the standard PSF is symmetric about the focal plane resulting in almost identical indistinguishable images for a single fluorescent molecule above and below the focal plane. Second, the standard PSF contains little information about the axial position of the emitter for a range of a few hundred nanometers near the focal plane.

Several imaging methods have been described which provide 3D SR information with widefield microscopy; astigmatism,[5] multiplane methods,[6] and interferometry.[7] We have recently demonstrated a powerful method for 3D imaging where the PSF of the microscope has been engineered to contain more information about the axial location of a point source. This so-called double-helix PSF (DH-PSF) has two lobes that spin around their midpoint throughout the depth of field, hence appearing as a double-helix along the axial dimension.[8] As a result, the image of a single point emitter appears as two lobes where the midpoint between the two lobes yields the lateral (i.e., x,y) position, and the angle between the two lobes with respect to a reference direction can be calibrated for estimation of the axial (i.e., z) position of a single emitter. The theoretical and experimental localization precisions of the DH-PSF quantitatively depend upon the inverse square root of the number of photons detected and the z position of the nanoscale emitter.[9] In this paper, by using a Fisher information calculation, we theoretically compare the best-case localization precision of the 3D DH-PSF approach to those for astigmatic and biplane imaging.[5,6] We show that for the same number of detected photons, the DH-PSF results in almost constant localization precision in all three dimensions over a large axial range whereas astigmatism and biplane perform well in limited axial ranges around the focal plane. Moreover, for experiments with a high signal-to-background ratio (SBR), the DH-PSF on average achieves better localization precision than the other two methods over a 2 μm depth of field.

In order to simulate each PSF as a probability distribution for photon detection, a requirement for calculation of the Fisher information content, computational models of each imaging system were developed. Figure 1 shows the key optical components of the collection optics for (a) the DH-PSF, (b) the astigmatic PSF, and (c) the biplane cases; the

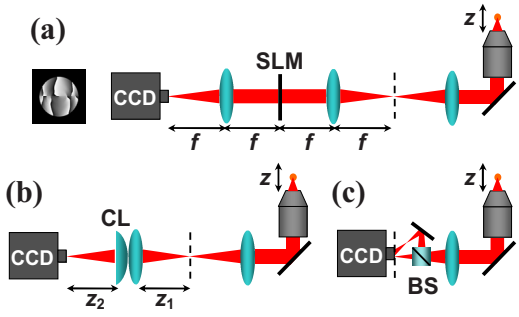

FIG. 1. (Color online) Schematic of the DH-PSF, astigmatic, and biplane imaging systems, where all three are implemented as additional image processing sections outside a standard microscope. (a) The DH-PSF setup uses a 4f imaging system with a phase-only SLM at the Fourier plane whose phase mask is the inverse Fourier transform of the DH-PSF. (b) The astigmatic setup is composed of a CL placed near a spherical lens. (c) The biplane setup uses a BS to modify the detection path for simultaneous imaging of two axially separated object planes.

a)Electronic mail: wmoerner@stanford.edu.

illumination optics in each case illuminate a large field of the sample. The DH-PSF setup [Fig. 1(a)] is composed of a standard epifluorescence microscope to which a $4f$ imaging system has been added with a liquid crystal phase-only spatial light modulator (SLM) in the focal plane of the first lens. Assuming that the numerical aperture of the system is sufficiently large, a point source one focal length in front of the first lens is Fourier transformed to a uniform plane wave in the SLM plane. This uniform distribution is multiplied by the phase mask of the SLM [Fig. 1(a) inset], which is then Fourier transformed again by the second lens onto the charge-coupled device (CCD) camera. The phase mask of the SLM was provided by R. Piestun and S. R. P. Pavani at the University of Colorado.[10]

In astigmatic imaging, asymmetry is added to the standard fluorescence image, and the orientation of the asymmetry is used to estimate z position of the emitter. To model the astigmatic PSF [Fig. 1(b)], a cylindrical lens (CL) is placed next to a spherical lens to map the image plane of the microscope onto the CCD. The CL results in an asymmetric quadratic phase along the x and y axes. Therefore, unlike a typical spherical lens which only has one focus, the combination of the CL and spherical lens has two foci, one along the x axis at one z position and one along the y axis at a displaced z position. The CCD is placed at the axial midpoint between these two foci.

In the biplane setup [Fig. 1(c)], the detection path of the standard microscope is modified to allow simultaneous imaging of two axially separated object planes. Z-position is estimated by fitting the images in both planes. In this scheme, a 50/50 beam splitter (BS) divides the incoming beam into a transmitted and a reflected beam and both are imaged onto different regions of the CCD.

In order to simulate the standard PSF of the microscope (which is common to all three approaches), a 100×, 1.4 numerical aperture oil-immersion objective (including the tube lens) is assumed. The refractive index of the oil is taken to be 1.518 and the wavelength of the light is 633 nm. For the DH-PSF we have assumed that all of the lenses in the $4f$ setup have the same focal length, $f=15$ cm, and that the SLM is a phase-only modulator with its size matching the back aperture size of the microscope objective. For the numerical simulation of the astigmatic PSF, we have matched our simulation parameters as closely as possible to the cases which have been implemented experimentally,[5,11] and take $f_{CL}=1$ m and $f_{SL}=4$ cm for focal lengths of the cylindrical and the spherical lens, respectively. This configuration results in ~600 nm distance between the two foci in the object space. For the biplane simulation, we have imaged two object planes that are ~300 nm above and below the original object plane in the standard microscope.[6,11] The three imaging setups have been designed to have the same overall magnification equal to $M=100$ of the standard microscope. All computations use scalar diffraction theory and a wave-optics analysis of the respective imaging system.[12]

The Fisher information matrix describes how much information a likelihood function contains about a parameter.[13] Here, the likelihood function is the PSF image and the parameters of interest are the lateral and axial positions of the emitter. The inverse of the Fisher information matrix is called the Cramer–Rao bound (CRB), which is the smallest possible position estimation variance that can be achieved with an unbiased estimator. The square root of the CRB is thus the lower limit of attainable localization precision. The CRB is especially useful for comparing different microscopy techniques. It is worth noting that Fisher information is a universal quantity that relies only upon the spatial variation rate of the PSF and is independent of the estimation algorithm. This simply means that a stronger variation in the PSF in any spatial dimension results in a larger value of Fisher information and consequently better (smaller) localization precision in that dimension.

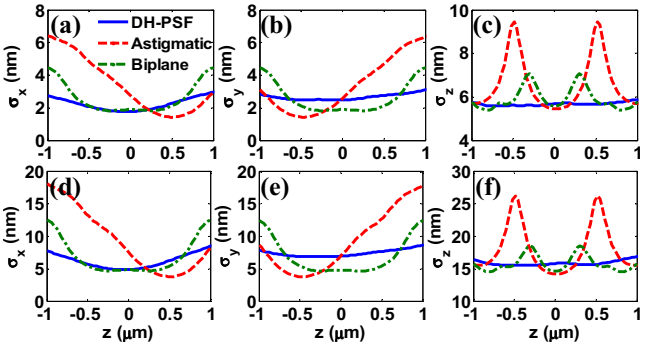

FIG. 2. (Color online) Comparison of the [(a) and (d)] x, [(b) and (e)] y, and [(c) and (f)] z localization precision among the DH-PSF, the astigmatic PSF, and the biplane for $N=6000$ (top panel) and $N=1000$ photons (bottom panel) detected on the CCD with 2 photons/pixel background level in each case. The DH-PSF has more uniform localization precision than the other two methods in all three dimensions.

In order to calculate the limit of the localization precision, we have adopted the methodology described previously[14,15] with the only difference being that the image function is replaced by the DH-PSF, the astigmatic PSF, and the biplane PSF. We have also included two important non-ideal effects in our calculation: pixelation due to finite-sized pixels of the CCD, and background fluorescence which arises from any fluorescent object that is not the emitter of interest, and which lowers the information due to its fluctuations. For a pixelated detector with additive background Poisson noise with mean β photons/pixel, the Fisher information matrix is as follows:

$$\mathbf{I}(\theta)=\sum_{k=1}^{N_p}\frac{1}{\mu_\theta(k)+\beta}\left[\frac{\partial\mu_\theta(k)}{\partial\theta}\right]^T\frac{\partial\mu_\theta(k)}{\partial\theta}\qquad\theta=(x_0,y_0,z_0)\in\Theta,$$

where μ_θ is the pixelated PSF image proportional to the number of detected photons N. Here Θ denotes the parameter space, (x_0,y_0,z_0) denotes the 3D location of the emitter in the object space, and N_p is the number of pixels. In all calculations below, we have assumed $N_p=625$ square pixels of effective width 160 nm at the sample plane (i.e., an array of 25×25 pixels is used to fully cover the significant region of the PSF). For the biplane case, the Fisher information is additive from the two image planes.

The DH-PSF, astigmatic PSF, and biplane have been separately compared with the standard PSF in the past and have shown superior behavior by removing the singularity in the axial localization precision.[16,17] Figure 2 compares x, y, and z localization precision of the DH-PSF with the astigmatic PSF and biplane as a function of the axial position z with respect to focus. The top panels of the figure [(a)–(c)] correspond to $N=6000$ and the bottom panels [(d)–(f)] to $N=1000$ photons detected on the CCD, both with $\beta=2$ photons/pixel. The DH-PSF has more uniform localiza-

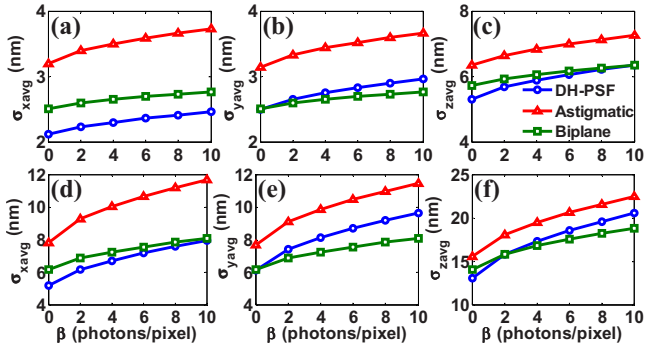

FIG. 3. (Color online) Comparison of the [(a) and (d)] x, [(b) and (e)] y, and [(c) and (f)] z averaged localization precision vs background level in photons/pixel among the DH-PSF, the astigmatic PSF, and the biplane for $N=6000$ (top panel) and $N=1000$ photons (bottom panel) detected on the CCD. For high SBR the DH-PSF is superior to the other two; however for low SBR, biplane achieves improved performance.

tion precision than the other two PSFs in all three dimensions throughout the whole 2 μm depth of field. This is a direct result of its almost constant spatial variation rate in all three dimensions, which makes it more suitable for 3D SR imaging of thicker samples. (In fact, for samples thicker than 2 μm, the entire PSF can be shifted in z if necessary by a proper phase adjustment of the SLM.) For the case with high SBR [$N=6000$ in Fig. 2(c)], the DH-PSF is superior to the other two PSFs in axial performance for all z. However for low SBR [$N=1000$ in Fig. 2(f)], the astigmatic PSF and biplane achieve better axial localization precision for smaller axial ranges around the focal plane. Beyond this range, their axial localization precisions are unsatisfactory, which effectively make them more suitable for thinner samples.

Figure 3 compares averaged x, y, and z localization precision of the three PSFs over the 2 μm depth of field as a function of background photons β. The top panels of the figure [(a)–(c)] correspond to high SBR ($N=6000$) and the bottom panels [(d)–(f)] to low SBR ($N=1000$). For high SBR, the DH-PSF outperforms the other two PSFs in the x and z dimensions and localizes as well as biplane in the y dimension. For low SBR, biplane is more suitable, especially in the axial dimension when background is significant [see Fig. 3(f)], although biplane and DH-PSF are generally comparable.

In conclusion, we have compared the best-case 3D localization precision with an unbiased estimator of the DH-PSF to the corresponding precisions of the astigmatic PSF and biplane using parameters matched as closely as possible to their actual implementations. The DH-PSF results in small and almost constant localization precision over a large axial range of ~2 μm, while for lower SBR situations, astigmatism and biplane achieve smaller axial localization precision in a shorter z range around the focal plane. Further, we have shown that for high SBR, the averaged axial localization precision of the DH-PSF is superior to the other two methods, while for low SBR biplane is preferable. All three methods can simply be integrated with the standard microscope to enable 3D PALM/STORM SR imaging. The direct and consistent comparison between the three methods shown in this paper should be useful to investigators needing to choose a scheme for 3D SR imaging in a specific case.

This work was supported in part by Grant No. R01GM085437 from the National Institute of General Medical Sciences. M.D.L. and M.A.T. acknowledge support from National Science Foundation Graduate Research Fellowships. M.D.L. is also supported by a 3Com Corporation Stanford Graduate Fellowship, and M.A.T. is also supported by a Bert and DeeDee McMurtry Stanford Graduate Fellowship.

[1] S. W. Hell, Nat. Methods **6**, 24 (2009).
[2] E. Betzig, G. H. Patterson, R. Sougrat, O. W. Lindwasser, S. Olenych, J. S. Bonifacino, M. W. Davidson, J. Lippincott-Schwartz, and H. F. Hess, Science **313**, 1642 (2006).
[3] S. T. Hess, T. P. K. Girirajan, and M. D. Mason, Biophys. J. **91**, 4258 (2006).
[4] M. J. Rust, M. Bates, and X. Zhuang, Nat. Methods **3**, 793 (2006).
[5] B. Huang, W. Wang, M. Bates, and X. Zhuang, Science **319**, 810 (2008).
[6] M. F. Juette, T. J. Gould, M. D. Lessard, M. J. Mlodzianoski, B. S. Nagpure, B. T. Bennett, S. T. Hess, and J. Bewersdorf, Nat. Methods **5**, 527 (2008).
[7] G. Shtengel, J. A. Galbraith, C. G. Galbraith, J. Lippincott-Schwartz, J. M. Gillette, S. Manley, R. Sougrat, C. M. Waterman, P. Kanchanawong, M. W. Davidson, R. D. Fetter, and H. F. Hess, Proc. Natl. Acad. Sci. U.S.A. **106**, 3125 (2009).
[8] S. R. P. Pavani, M. A. Thompson, J. S. Biteen, S. J. Lord, N. Liu, R. J. Twieg, R. Piestun, and W. E. Moerner, Proc. Natl. Acad. Sci. U.S.A. **106**, 2995 (2009).
[9] M. A. Thompson, M. D. Lew, M. Badieirostami, and W. E. Moerner, Nano Lett. **10**, 211 (2010).
[10] S. R. P. Pavani and R. Piestun, Opt. Express **16**, 3484 (2008).
[11] M. J. Mlodzianoski, M. F. Juette, G. L. Beane, and J. Bewersdorf, Opt. Express **17**, 8264 (2009).
[12] J. W. Goodman, *Introduction to Fourier Optics*, 3rd ed. (Roberts & Company, Greenwood Village, CO, 2005).
[13] T. M. Cover and J. A. Thomas, *Elements of Information Theory*, 2nd ed. (Wiley, New York, 2006).
[14] R. J. Ober, S. Ram, and E. S. Ward, Biophys. J. **86**, 1185 (2004).
[15] S. Ram, P. Prabhat, J. Chao, E. S. Ward, and R. J. Ober, Biophys. J. **95**, 6025 (2008).
[16] S. R. P. Pavani and R. Piestun, Opt. Express **16**, 22048 (2008).
[17] C. v. Middendorff, A. Egner, C. Geisler, S. W. Hell, and A. Schönle, Opt. Express **16**, 20774 (2008).